



HAL
open science

Effective transport barriers in the biquadratic nontwist map

Gabriel C. Grime, Ricardo L. Viana, Yves Elskens, Iberê Caldas

► **To cite this version:**

Gabriel C. Grime, Ricardo L. Viana, Yves Elskens, Iberê Caldas. Effective transport barriers in the biquadratic nontwist map. 2024. hal-04693584

HAL Id: hal-04693584

<https://hal.science/hal-04693584v1>

Preprint submitted on 10 Sep 2024

HAL is a multi-disciplinary open access archive for the deposit and dissemination of scientific research documents, whether they are published or not. The documents may come from teaching and research institutions in France or abroad, or from public or private research centers.

L'archive ouverte pluridisciplinaire **HAL**, est destinée au dépôt et à la diffusion de documents scientifiques de niveau recherche, publiés ou non, émanant des établissements d'enseignement et de recherche français ou étrangers, des laboratoires publics ou privés.



Distributed under a Creative Commons Attribution - NonCommercial - ShareAlike 4.0 International License

Effective transport barriers in the biquadratic nontwist map

Gabriel C. Grime,¹ Ricardo L. Viana,^{2,3} Yves Elskens,⁴ and Iberê L. Caldas¹

¹*Institute of Physics, University of São Paulo, São Paulo 05508-090, Brazil*

²*Physics Department, Federal University of Paraná, Paraná 81531-990, Brazil*

³*Centro Interdisciplinar de Ciência, Tecnologia e Inovação, Núcleo de Modelagem e Computação Científica, Federal University of Paraná, Paraná 81530-000, Brazil*

⁴*Aix-Marseille Université, UMR 7345 CNRS, PIIM, campus Saint-Jérôme case 322, 13397 Marseille cx 13, France*

(*Electronic mail: gabrielgrime@gmail.com)

(Dated: 4 September 2024)

Nontwist area-preserving maps violate the twist condition at specific orbits, resulting in shearless invariant curves that prevent chaotic transport. Plasmas and fluids with nonmonotonic equilibrium profiles may be described using nontwist systems, where even after these shearless curves breakdown, effective transport barriers persist, partially reducing transport coefficients. Some nontwist systems present multiple shearless curves in phase space, increasing the complexity of transport phenomena, which have not been thoroughly investigated until now. In this work, we examine the formation of effective transport barriers in a nontwist area-preserving mapping with multiple shearless transport barriers. By quantifying the effectiveness of each transport barrier in phase space, we identified two scenarios where particular barriers dominate over others. Our results also reveal configurations where the interplay of two transport barriers creates regions in phase space with significant orbit trapping, thereby influencing the overall transport dynamics.

I. INTRODUCTION

Transport phenomena play a fundamental role in nature and involve redistributing quantities such as particles, charge, and energy. Different mechanisms are responsible for transport processes, which can explain phenomena ranging from microscopic interactions in semiconductors¹ to large-scale planetary dynamics².

In dynamical systems, the problem of transport involves quantifying the collective motion of an ensemble of orbits between regions in phase space³. Hamiltonian systems often represent models of physical significance, such as fluid advection^{4,5} and magnetically confined plasmas⁶⁻⁹. Featuring a mixed phase space, Hamiltonian dynamics exhibit periodic, quasiperiodic, and chaotic trajectories, with chaotic trajectories being responsible for transport¹⁰.

The intermixing of regular and chaotic orbits in phase space complicates the transport problem in Hamiltonian systems. Certain structures in phase space can reduce or even eliminate chaotic transport. For instance, quasiperiodic invariant curves act as total barriers, eliminating transport through them¹¹. Therefore, the breakup of the last invariant curve is of great importance, and in twist systems, the Kolmogorov-Arnold-Moser (KAM) theorem addresses this issue¹².

Nontwist systems violate the twist condition at some orbits, forming the so-called shearless invariant curves. Although the KAM theorem is not valid in these maps, analytical and numerical results indicate that the shearless invariant curve is among the last invariant tori to break up^{13,14}. Furthermore, nontwist systems have degenerate Hamiltonians, leading to new topological processes involving isochronous island chains, for example, periodic orbit collision and separatrix reconnection^{15,16}.

Even after their breakdown, remnants of invariant curves, including the shearless, can reduce transport coefficients in the region, forming a partial or effective transport barrier³.

Furthermore, the effectiveness of these barriers is closely related to the inter-intracrossing nature of manifolds associated with periodic island chains¹⁷⁻²⁰.

Nontwist dynamics appears in various research areas, including fluid advection^{5,21}, geophysical zonal flows²², and magnetically confined plasmas^{23,24}.

Professor R. L. Dewar was among the pioneers in applying area-preserving maps to the study of magnetically confined plasmas. He utilized the Hamiltonian formalism to investigate magnetic island structures within the Helic stellarator. Building on previous research²⁵, he compared nontwist Hamiltonian models with reversed shear stellarator data, revealing their similarities²⁶. This work, along with several other studies²⁷⁻²⁹, significantly advanced the understanding of area-preserving maps and their application to tokamaks^{30,31}.

Nontwist area-preserving maps have been used to investigate the general properties of such systems. The Standard Nontwist Map, for example, is a paradigmatic system that captures the essential behavior of systems that violate the twist condition at one single orbit¹⁴. Consequently, many works on effective transport barriers in nontwist systems have utilized this map^{18-20,32,33}.

Recently, experimental evidence has indicated the existence of more than one transport barrier in nonmonotonic plasma equilibrium³⁴. Additionally, plasma-transport models have utilized nontwist systems to explain transport reduction³⁵⁻³⁷. In such nontwist systems, more than one orbit violates the twist condition, leading to complex nontwist processes with unique characteristics, such as reconnection-collision sequences^{16,38}. Recently, the Biquadratic Nontwist Map has been used to study bifurcation processes and shearless curve breakdown in systems with multiple shearless curves^{39,40}. However, there has been no study so far on how multiple effective barriers influence transport in phase space.

In this work, we investigate the formation of an effective transport barrier in the Biquadratic Nontwist Map, a prototype system with multiple shearless transport barriers. Using com-

putational and theoretical tools, we quantify the effectiveness of each barrier individually. Our results revealed scenarios where a specific barrier dominates over the others. Furthermore, the presence of two transport barriers can create chaotic regions where orbits remain trapped for extended periods.

The rest of the paper is organized as follows. Section II presents the area-preserving map used in our analysis. The theoretical background about transport analysis tools and quantifiers is provided in Section III. Section IV applies these quantifiers to the Biquadratic Nontwist Map, exploring how multiple transport barriers affect low and high transport configurations. Finally, Section IV offers our conclusions.

II. MULTIPLE SHEARLESS CURVE SYSTEMS

Let us consider a two-dimensional area-preserving map with a particular functional form, defined by the recurrence relations

$$x_{n+1} = x_n + \omega(y_{n+1}) \pmod{1} \quad (1a)$$

$$y_{n+1} = y_n - f(x_n), \quad (1b)$$

where $x \in [0, 1)$ and $y \in \mathbb{R}$ are a pair of canonical coordinate and momentum. Its phase space is the infinite cylinder $\mathbb{S}^1 \times \mathbb{R}$. Functions f and ω must be sufficiently differentiable. Additionally, for such a system to be used as a model for studying Hamiltonian dynamics, we require f to be a period-1 function with zero average¹⁰.

The twist function ω gives the frequency of the orbits in phase space when the system is integrable, i.e., when $f(x) \equiv 0$. If ω has no extreme point, the map (1) is called a twist map, and satisfies the condition

$$\left| \frac{\partial x_{n+1}}{\partial y_n} \right| = |\omega'(y_{n+1})| > 0 \quad (2)$$

for every point in phase space⁴¹.

Maps that do not satisfy the twist condition are called nontwist maps. Consequently, important results, such as the Kolmogorov-Arnold-Moser (KAM) theorem, are not valid⁴². Significant nontwist systems, such as the Standard Nontwist Map, violate the twist condition at only one point¹⁴. However, general maps might violate the twist condition at multiple points, thereby increasing the complexity of nontwist phenomena presented, such as reconnection of separatrices⁴³.

A. The Biquadratic Nontwist Map

It is suitable to use specific functional forms of ω and f for the resultant map to possess useful properties. By choosing the twist function $\omega(y) = a(1 - y^2)(1 - \epsilon y^2)$ and the perturbation $f(x) = b \sin(2\pi x)$, we obtain the Biquadratic Nontwist Map (BNM)³⁹:

$$x_{n+1} = x_n + a(1 - y_{n+1}^2)(1 - \epsilon y_{n+1}^2) \pmod{1} \quad (3a)$$

$$y_{n+1} = y_n - b \sin(2\pi x_n). \quad (3b)$$

When $b = 0$, the phase space contains only periodic and quasiperiodic ($y = \text{constant}$) orbits. Near integrability occurs for small perturbation parameters ($b \ll 1$). Typical phase spaces of the BNM in this regime are shown in Fig. 1. In this case, periodic orbits give rise to resonance islands, and the quasiperiodic invariant curves become distorted.

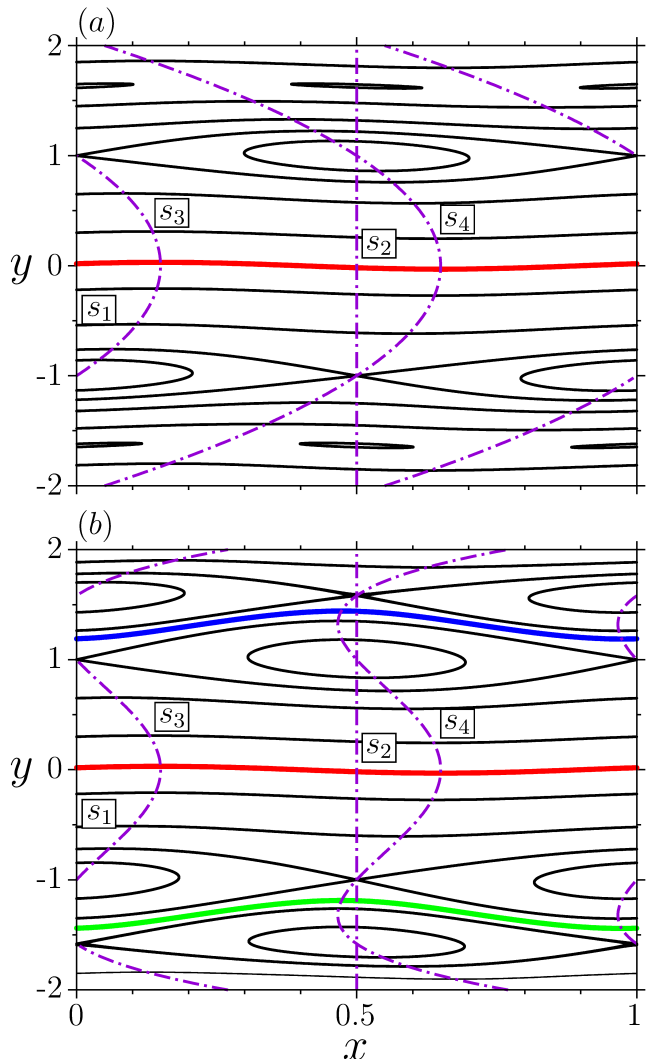


FIG. 1. Phase spaces of the Biquadratic Nontwist Map, with $a = 0.3$ and $b = 0.05$, (a) $\epsilon = 0$ and (b) $\epsilon = 0.4$. Symmetry lines are marked by dashed-dotted lines, while shearless curves appear in red, blue, and green lines.

The BNM is a nontwist map because its twist function violates the twist condition, Eq. (2). For $\epsilon > 0$, the map exhibits three such orbits, known as shearless invariant sets

$$\mathcal{R}_0 : y = b \sin(2\pi x) \quad (4a)$$

$$\mathcal{R}_{\pm} : y = \pm \sqrt{\frac{1 + \epsilon}{2\epsilon}} + b \sin(2\pi x), \quad (4b)$$

defined by the regions in phase space that violate the twist condition⁴⁴. In this paper, we will call \mathcal{C}_0 the central shearless

curve, associated with \mathcal{R}_0 . The same occurs to \mathcal{C}_\pm , named external shearless curves, intersecting \mathcal{R}_\pm .

In Fig. 1(b), the red curve stands for the \mathcal{C}_0 , while \mathcal{C}_\pm are marked in blue and green. For $\varepsilon = 0$, Fig. 1(a), the BNM twist function is parabolic and, in this case, the Biquadratic Nontwist Map reduces to the Standard Nontwist Map¹⁴ (SNM), which has only a central shearless curve.

Notice that the BNM has symmetry properties concerning time evolution and spatial transformation. The time evolution symmetry leads to the symmetry lines s_i , $i = 1, 2, 3, 4$, useful to find periodic orbits⁴⁵. For example, the symmetry lines intersections correspond to the map's fixed points. Those lines are marked by dashed-dotted lines in Fig. 1. Furthermore, the map is symmetric under the spatial transformation $S(x, y) = (x + 1/2, -y)$; therefore, the behavior of orbits is equivalent above and below the central shearless curve \mathcal{C}_0 . For example, the external shearless curves and the period-1 resonance islands are symmetrical under S . Although the external shearless curves are symmetric, i.e., \mathcal{C}_+ is symmetric to \mathcal{C}_- , the map is not symmetrical with respect to them.

The BNM has been used in previous studies concerning nontwist systems with multiple shearless curves. Due to its symmetry properties and the range of phenomena displayed, it serves as a useful model for studying general nontwist systems, that present multiple shearless curves. Further characterization and results about the BNM can be found in Ref. 39 and 40.

B. Effective transport barriers

Away from integrability, the BNM exhibits a mixed-type phase space. Alongside regular orbits (resonances and invariant curves), irregular (chaotic) orbits fill nonzero volume regions in phase space, as depicted in Fig. 2(a). These irregular orbits lead to chaotic transport, i.e., the motion of a collection of trajectories across different regions of phase space. As the perturbation parameter grows, invariant curves are broken, causing chaos to spread throughout phase space. The remaining invariant curves serve as barriers to transport, delineating boundaries for chaotic orbits. Consequently, once the last curve is broken, chaotic orbits traverse all available space, leading to a scenario known as global transport.

Invariant curves are total transport barriers since they completely prevent transport along the momentum variable. However, even after their breakup, transport in the region is not diffusive. The remnants of the last invariant curve lead to a reduction in transport coefficients at the region. Such a reduction is attributed to long-time correlation functions, a signature of chaotic orbits wandering along the transport barrier in a phenomenon called stickiness⁴⁶. These remnants and their influence on transport have been studied on twist^{3,11} and nontwist systems^{18,20,32,33}.

Concerning nontwist systems, both analytical and numerical evidence suggest that the shearless curve is one of the last invariant curves to be broken^{13,14}. In addition, the arrangement of island chains around the shearless transport barrier plays a crucial role in the effectiveness of these partial

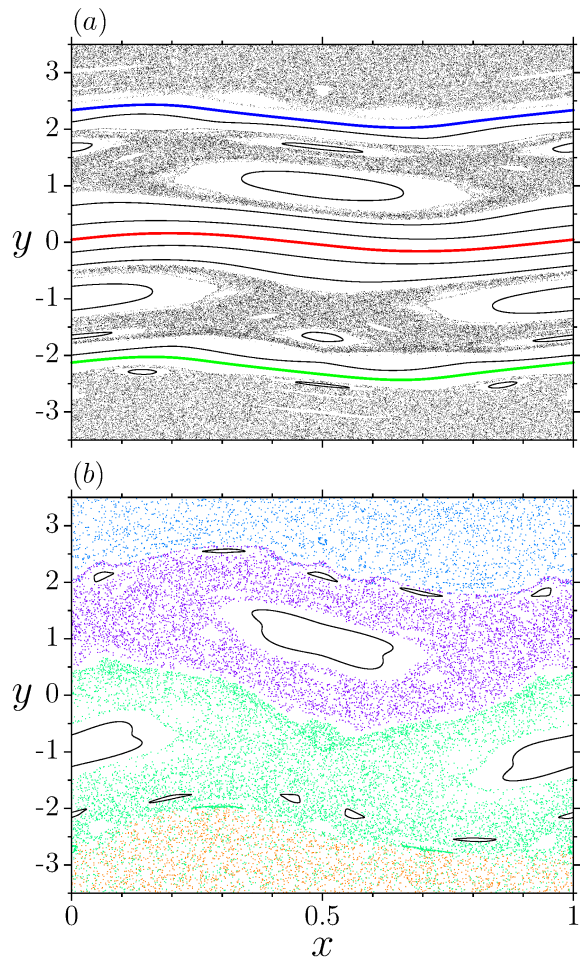


FIG. 2. Phase spaces of the Biquadratic Nontwist Map for $\varepsilon = 0.11$, (a) with $a = 0.4$ and $b = 0.3$, and (b) $a = 0.25$ and $b = 0.7906$. A partial barrier persists once a shearless curve is broken, preventing transport between the four regions of phase space, marked by chaotic orbits of different colors.

barriers^{20,22}.

The Biquadratic Nontwist Map has three shearless curves that break up in different configurations, with the central and external transport barriers breaking up independently⁴⁰. Still, there are parameter sets where all shearless curves are broken.

In the BNM, orbits can mix between four distinct regions in phase space. Figure 2(b) illustrates such a situation, where we evolved a unique orbit in each region of phase space. These four orbits are colored as follows: (i) above the top shearless transport barrier (blue), (ii) between the top and central barriers (purple), (iii) between the central and lower barriers (green), and (iv) below the lower barrier (orange). Initially, these orbits are trapped between the barriers. Yet, they eventually cross the barrier, causing mixing between regions of different colors.

III. TRANSPORT ANALYSIS FRAMEWORK

This section describes the methods used in this paper to investigate transport in the Biquadratic Nontwist Map (BNM). Some dynamical quantifiers have been used to evaluate transport properties in Hamiltonian systems. In this paper, we adopt the transmissivity of a transport barrier, escape time phase space and manifold analysis.

A. Transmissivity

The transmissivity measures the effectiveness of a given transport barrier in preventing orbits from crossing a given region in phase space. In other words, it quantifies the strength of a transport barrier. Given a set of initial conditions, we define the transmissivity of a barrier as the fraction of orbits that cross the same barrier. To numerically obtain this fraction, we define the circles

$$\partial\mathcal{B}_{\pm} = \{(x, y) \in \mathbb{S}^1 \times \mathbb{R} : 0 \leq x < 1, y = \pm y_B\}, \quad (5)$$

in phase space, where y_B is a constant value. Computationally, we randomly choose a large number of initial conditions on the circle $\partial\mathcal{B}_-$, which are iterated N times. The fraction of orbits that reach the circle $\partial\mathcal{B}_+$ is assigned as the transmissivity of the partial transport barrier inside the region bounded by $\partial\mathcal{B}_{\pm}$. Therefore, the value of y_B determines which barriers of the BNM are considered, as discussed in the next section.

A total transport barrier, which completely prevents the transport of orbits through it, has zero transmissivity. Shearless curves are examples of total transport barriers. Transmissivity values marginally greater than zero indicate a strong transport barrier, while values closer to one indicate a weak capability of preventing transport. Applying transmissivity for the BNM requires a careful choice of y_B , as this determines which transport barrier is considered. Results concerning transmissivity in the BNM are presented in Fig. 3, 4 and 8.

B. Escape time phase space

The escape time of trajectories in phase space can be used to investigate the stickiness of orbits on partial transport barriers. While transmissivity provides relevant information, it does not offer any data on the characteristic time scales associated with the transport barrier. Therefore, determining the time required for an orbit to escape a certain region of phase space allows us to verify the time that orbits spend in each region of phase space. This tool helps identify regions of stickiness and escape channels through which orbits leave the transport barrier.

In this work, the escape time phase space is obtained by setting a regularly spaced grid of 2000×2000 initial conditions, which are iterated a maximum of $2 \cdot 10^6$ times. We compute the number of iterations needed for the orbits to exit a certain region of phase space \mathcal{B} , bounded by $\partial\mathcal{B}_{\pm}$, previously defined. The choice of the constant y_B , which defines the region

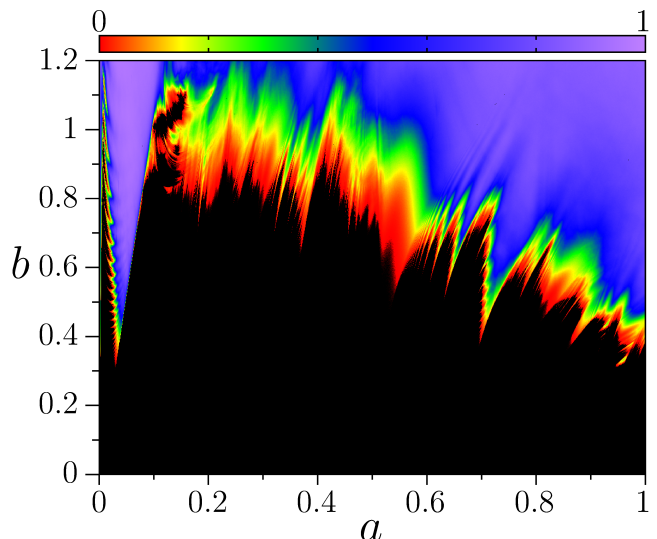


FIG. 3. Transmissivity parameter space of the Biquadratic Nontwist Map, fixed $\varepsilon = 0.11$. Colors represent the barrier transmissivity, with black being the zero transmissivity.

boundary, determines the transport barrier being considered. Results of the escape time phase space are shown in Figures 5, 6, 9 and 10.

C. Stable and unstable manifolds

Here, we provide a brief introduction to invariant manifolds in dynamical systems. Since this work focuses on the Biquadratic Nontwist Map, we restrict our discussion to two-dimensional area-preserving maps.

Let P be a hyperbolic period- p orbit of a two-dimensional area-preserving map $M : z \mapsto M(z)$, whose inverse is M^{-1} . Invariant manifolds are defined as the set of points in phase space that asymptotically accumulate on a given hyperbolic periodic orbit in at least one direction of time. Mathematically, the stable manifold W_s^P and the unstable manifold W_u^P associated with the hyperbolic orbit P are defined as

$$W_s^P = \{z \in D : M^n(z) \rightarrow P, n \rightarrow \infty\} \quad (6a)$$

$$W_u^P = \{z \in D : M^{-n}(z) \rightarrow P, n \rightarrow \infty\}, \quad (6b)$$

where $D = \mathbb{S}^1 \times \mathbb{R}$ is the domain of the map. In the context of our study, $W_{s,u}^P$ are one-dimensional curves. The computational method to obtain such invariant sets starts by choosing an appropriate linear segment, whose direction is given by the eigenvectors of the associated hyperbolic orbit. This segment is then evolved under the map dynamics to obtain the unstable manifold and under its inverse to obtain the stable manifold⁴⁷.

Locally, the manifolds of a map give the direction of the tangent space, indicating the direction in which nearby orbits evolve. Furthermore, the configuration of the stable and unstable manifolds of hyperbolic orbits determines the behavior of chaotic orbits and, consequently, transport in phase space.

IV. SCENARIOS OF DOMINANT TRANSPORT BARRIERS

This section examines how multiple transport barriers in the Biquadratic Nontwist Map (BNM) influence transport in phase space. Using the techniques described in the previous section, we explore how the central and external transport barriers impact low and high transport scenarios on the map.

Since the BNM features three independent shearless transport barriers, we can study the effect of each barrier individually or their combined effect. Regarding the last case, the boundaries $\partial\mathcal{B}_\pm$ (defined in Eq. (5)) must extend beyond the external shearless transport barriers. Conversely, to isolate the effect of the central transport barrier, the same boundaries must be placed between the central and external barriers.

In our analysis, we fix $\varepsilon = 0.11$. For this value, the central and external barriers do not intertwine, simplifying their individual analysis. Details about the typical phase space of the BNM in this configuration are shown in Figures 2 and 5. The external transport barriers, defined by Eq. (4), are located within the region $|y| \lesssim 3.35$. Therefore, choosing $y_B = 5$ ensures the boundaries $\partial\mathcal{B}_\pm$ are beyond the external shearless barriers. In contrast, to focus on the transmissivity of the central barrier alone, we set $y_B = 1.5$, positioning the boundaries between the central and external shearless barriers.

Taking into account the effect of all three shearless transport barriers, we illustrate the dependence of transmissivity on the parameters of the BNM in Figure 3. We computed the transmissivity using the method outlined in section III A, with a total of 10^4 initial conditions, iterated 10^4 times, considering boundaries $\partial\mathcal{B}_\pm$ where $y_B = 5$.

Black regions in parameter space have zero transmissivity, i.e., the phase space has at least one invariant curve acting as a total transport barrier. Further details on the scenarios with total transport barrier in the BNM can be found in Ref. 40.

According to the transmissivity parameter space, Figure 3, transport is still reduced after all invariant curves have broken. Regions with zero transmissivity are surrounded by low-transport zones, indicating that transport remains low immediately after the shearless curve breakdown. Additionally, there is a noticeable sensitivity of transmissivity to the map parameters, which can vary gradually or abruptly depending on the region of the parameter space.

Abrupt changes in transmissivity are attributed to topological modifications in the remnants of the transport barriers¹⁷. Furthermore, in the BNM, those changes can be associated with modification of the central or external transport barrier. The first scenario is named the *centrally dominant* transport barrier, while the last is the *externally dominant* transport barrier. The characterization of the topological changes in both dominant scenarios is detailed below.

A. Centrally dominant

In the centrally dominant scenario, nontwist processes involving the central transport barriers dictate the effectiveness of transport in the BNM. We compare the transmissivity when

considering only the central barrier ($y_B = 1.5$) versus considering all the barriers ($y_B = 3.5$). Figure 4 displays the transmissivity as a function of a , with fixed values of b and ε . Here, the transmissivity is obtained using an ensemble of 10^5 initial conditions iterated 10^6 times, or until they reach the boundary at $y = y_B$.

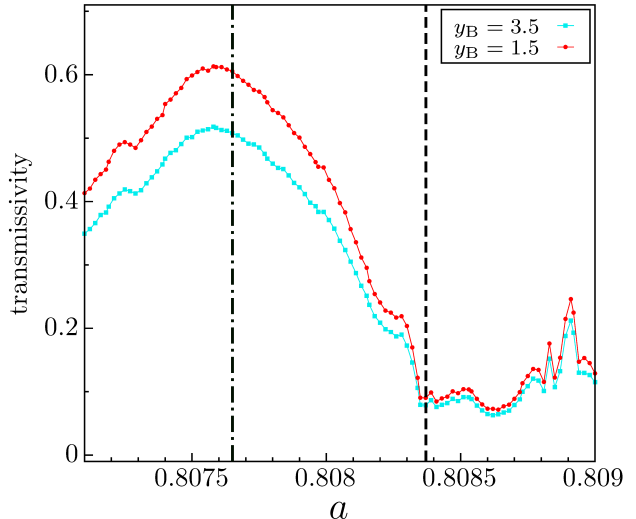


FIG. 4. Transmissivity of the Biquadratic Nontwist Map, as function of a , fixed $b = 0.58$ and $\varepsilon = 0.11$. Dashed-dotted and dashed lines mark high and low transport configurations, respectively.

We observe an abrupt change in transmissivity for both values of y_B . Two specific values of a are highlighted: the dashed line marks a low transmissivity configuration, while the dashed-dotted line marks a high transmissivity one. The results indicate that both low and high transport regimes are evident for the two values of y_B . Additionally, the transmissivity considering all transport barriers is slightly smaller compared to the effect of the central barrier alone. Briefly, in the centrally dominant scenario, transmissivity is primarily influenced by the central transport barrier. The external barriers tend to reduce transport, but their effect is minimal, especially in regions of low transmissivity.

Figure 5 shows the number of iterations needed for an orbit to escape the region of phase space bounded by $\partial\mathcal{B}_\pm$, where $y_B = 3.5$. The parameters used correspond to high [Fig. 5(a)] and low [Fig. 5(b)] transmissivity configurations from Figure 4. In both configurations, all invariant curves were destroyed, resulting in all chaotic orbits eventually escaping. However, the required time for these escapes greatly varies.

In both high and low transmissivity scenarios, most orbits escape after 10^3 iterations, particularly in the region bounded by $y \approx \pm 2$. Outside this portion of phase space, orbits typically take around 10 iterations to escape. The region where the escape time changes abruptly delineates the external partial transport barriers. Despite having different transmissivity values, Figures 5(a) and 5(b) do not show significant differences in escape times.

Computing the escape time to $y_B = 1.5$, which lies between

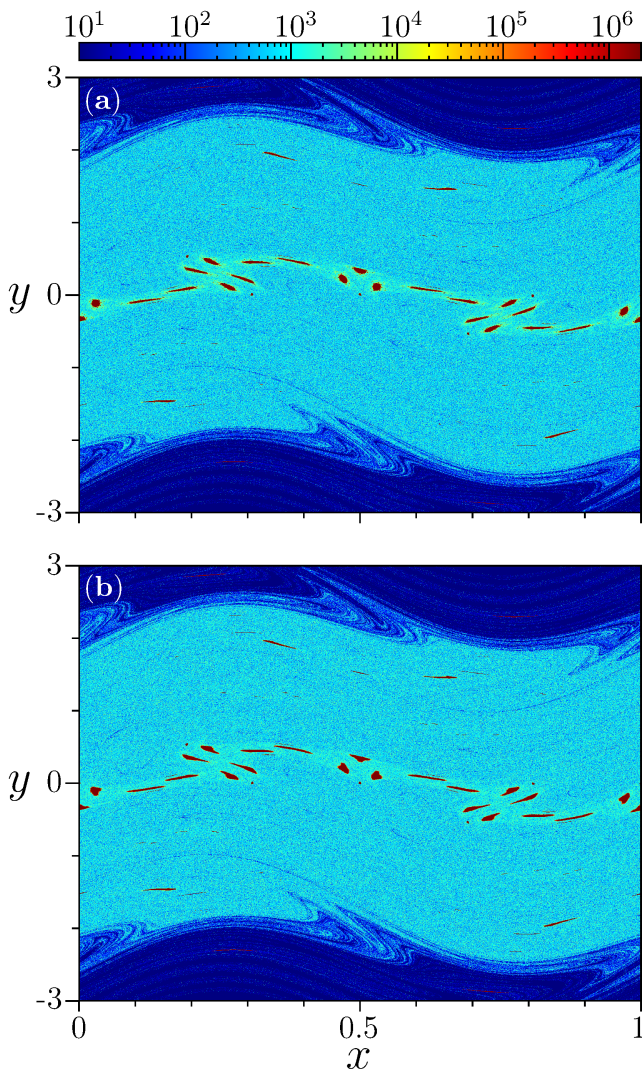


FIG. 5. Escape time of the trajectories in phase space of the Bi-quadratic Nontwist Map, with $b = 0.58$, $\varepsilon = 0.11$, (a) $a = 0.80765$ and (b) $a = 0.80837$, corresponding to high and low transport configurations of Fig. 4. Here we considered $y_B = 3.5$.

the central and external barriers, Figure 6 shows a phase space with a considerably different escape time distribution. The central transport barrier is formed by a pair of period-11 twin island chains embedded in the chaotic sea. Points inside these islands do not escape since they correspond to invariant sets. However, examining the escape times near the islands (highlighted rectangles in Figure 6), we observe that orbits adjacent to them linger longer than the rest of the chaotic orbits.

In some way, these adjacent orbits resemble the periodic behavior of the islands, causing them to remain trapped in the region for extended periods. This dynamical trap of orbits, called stickiness, has been studied in both twist³ and nontwist systems²⁰.

A detailed examination of Figures 6(a) and 6(b), which correspond to high and low transmissivity, indicates distinct escape times nearby the islands. In the low transmissivity scenario, sticky orbits require approximately 10^5 iterations to es-

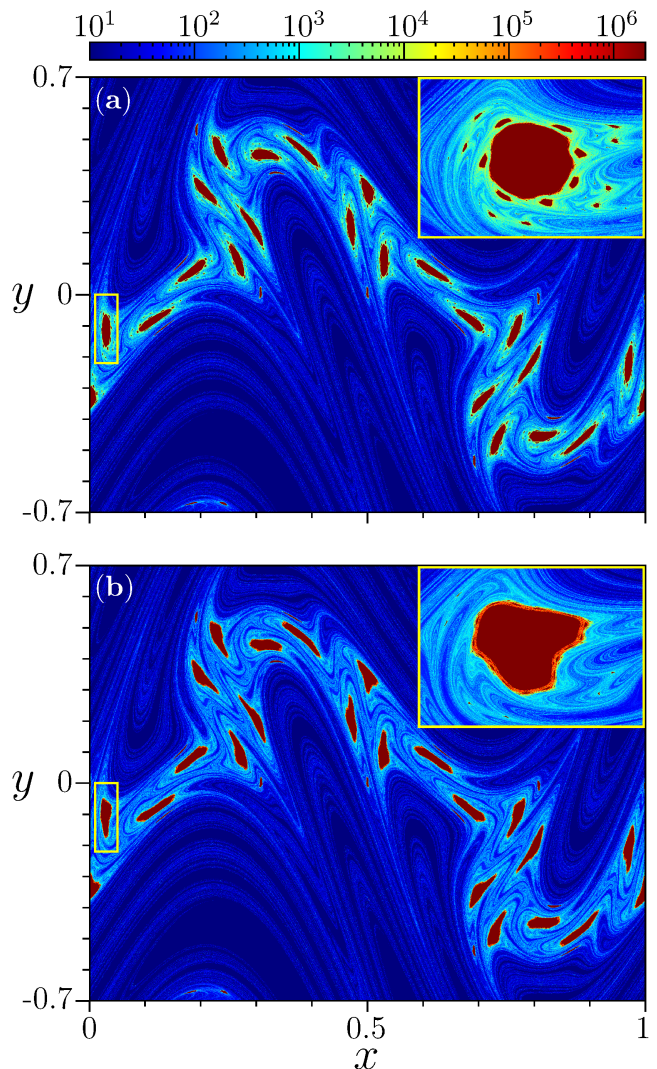


FIG. 6. Escape time near the central transport barrier of the Bi-quadratic Nontwist Map for (a) high and (b) low transmissivity regimes of Fig. 8, considering $y_B = 1.5$. Magnifications of the highlighted regions are embedded in the corresponding panels.

cape the central region, whereas in the high transmissivity, they take only about 10^4 iterations. Notably, for the same parameters, the escape times considering the external transport barriers remain roughly the same (see Fig. 5). Therefore, the escape time analysis also indicates the dominance of the central barrier over the external ones in this scenario.

As defined in section III, manifolds dictate the behavior of orbits in phase space. According to the Poincaré-Birkhoff theorem, island chains originate from a pair of stable and unstable periodic orbits⁴². In turn, each unstable periodic orbit has a stable and an unstable hyperbolic manifold. Specifically, the island chains in the central transport barrier are denoted as the upper and lower chains. The hyperbolic period-11 orbit of the upper (lower) chain is marked by filled squares (triangles) and denoted by U (L) in Figure 7. The corresponding stable and unstable manifolds are denoted by W_s^U (W_s^L) and W_u^U (W_u^L).

The six panels of Figure 7 are divided as follows. The upper

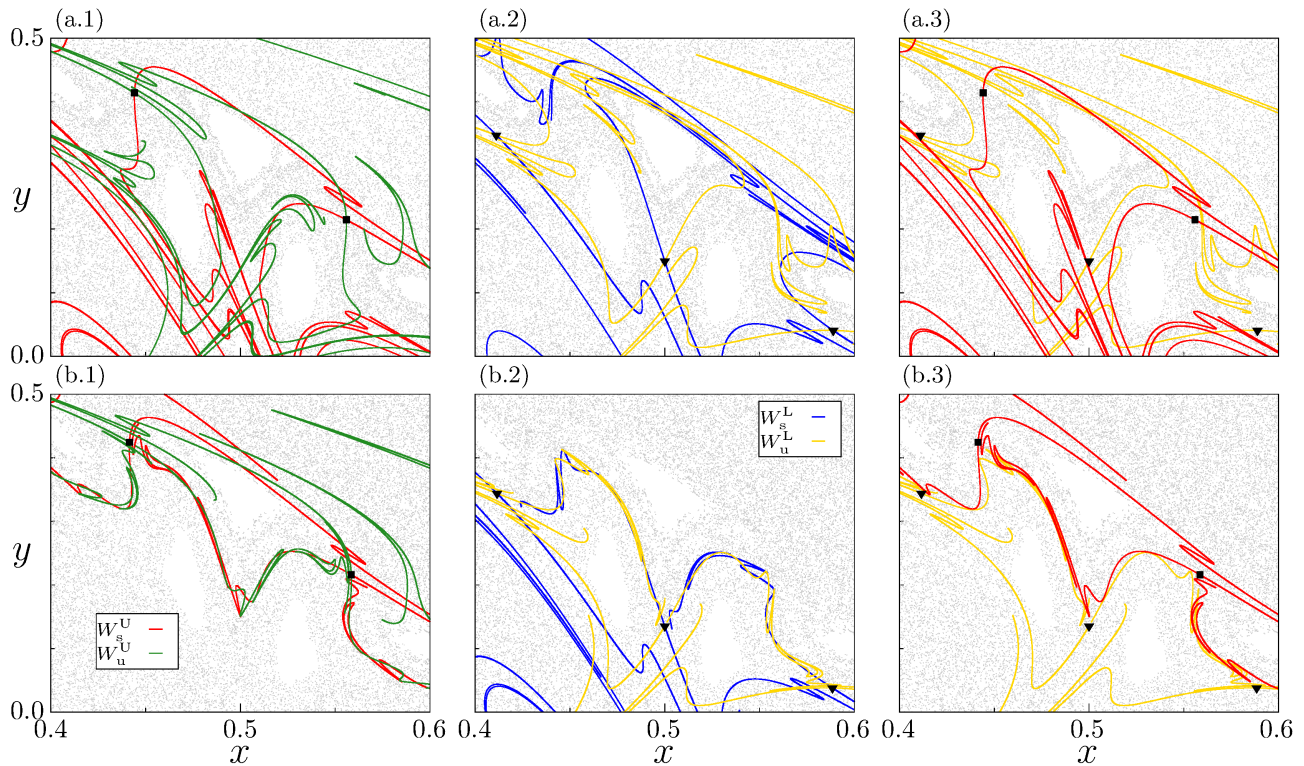


FIG. 7. Stable and unstable manifolds of the upper (W_s^U and W_u^U) and lower (W_s^L and W_u^L) periodic orbit, considering (a) high and (b) low transport configurations of Fig. 4. Chaotic orbits near them are plotted in light-grey.

panels refer to the high transmissivity, while the lower panels correspond to the low transmissivity regime. The left (central) panels show the manifolds associated with the upper (lower) periodic orbit, while the right panels exhibit stable and unstable manifolds of different periodic orbits.

The stable and unstable manifolds associated with upper and lower orbits intersect in a complex structure, determining the motion of chaotic orbits and transport. Manifolds of the same hyperbolic orbit intersect in a structure called homoclinic tangle (see, for example, Figs. 7(a.1) and 7(b.1)). These intersections are named *intracrossing* and the emergence of chaos in Hamiltonian systems is closely related to them⁴¹. However, nontwist systems also present *intercrossing*, i.e., the intersection of manifolds associated with different hyperbolic orbits, creating the heteroclinic tangle responsible for the effectiveness of nontwist transport barriers²⁰.

The turnstile mechanism explains how island chains act as transport barriers based on the intercrossing structure of the stable and unstable manifolds. Fundamentally, the regions through which orbits enter and leave the resonance zone, called lobes, dictate the effectiveness of such a transport barrier. A lobe is a region between two consecutive intersections of the stable and unstable manifolds of a given periodic orbit. In summary, the mechanism asserts that transport is directly connected to lobe size: high transport occurs with large lobe size, while low transport is associated with small lobes.

In the BNM, the homoclinic tangle differs significantly between the low and high transport configurations shown in Figure 7. The lobe sizes are considerably larger in the high

transport regime [Figs. 7(a.1) and 7(a.2)] compared to the low transmissivity configuration [Figs. 7(b.1) and 7(b.2)]. In high transport regime, orbits can easily enter and leave the resonance zone, as stated by the turnstile mechanism. Finally, due to the symmetry of the BNM, lobe sizes of manifolds related to both upper and lower orbits are similar, resulting in equal upward and downward transport.

The other transport mechanism, relevant in nontwist systems, is the intercrossing of manifolds. As detailed in Ref.²⁰, the intersections of manifolds from different (but closer) chains form escape channels used by orbits to leave the transport barrier region. In the high transport regime [Figure 7(a.3)] there is a large number of those intercrossings compared to low transmissivity, Fig. 7(b.3). These intercrossings occur because W_s^U (W_u^L) intertwine with the lower (upper) island chain, resembling a homoclinic topology of separatrices.

We stress that both the turnstile mechanism and intercrossing are complementary in describing transport in nontwist systems¹⁸. The intercrossing and turnstile mechanism dictates how orbits enter and leave the resonance zone of a specific island chain. However, since nontwist transport barriers are formed by a pair of island chains, the intercrossing of manifolds governs how orbits transition between these island chains.

The manifold structure also dictates the escape channels through which orbits leave the sticky region³¹. A detailed look at Figure 6 exhibits incursions of low escape time (dark blue) among regions with significantly large escape times (light blue and green). Since the escape channels coincide with the lobes,

these incursions are directly connected with the manifold behavior shown in Figure 7.

B. Externally dominant

In the externally dominant scenario, processes involving the external transport barriers determine the transport properties in the Biquadratic Nontwist Map (BNM). Figure 8 shows the transmissivity of the BNM as a function of the parameter a , considering the effect of all transport barriers combined ($y_B = 3.5$). Here, we observe a sudden change in the transmissivity, just like in Figure 4. The configuration of low (high) transmissivity is marked by a dashed (dashed-dotted) line. As we will see, in both scenarios, the central barrier does not significantly affect the transport; only the external barriers play an important role.

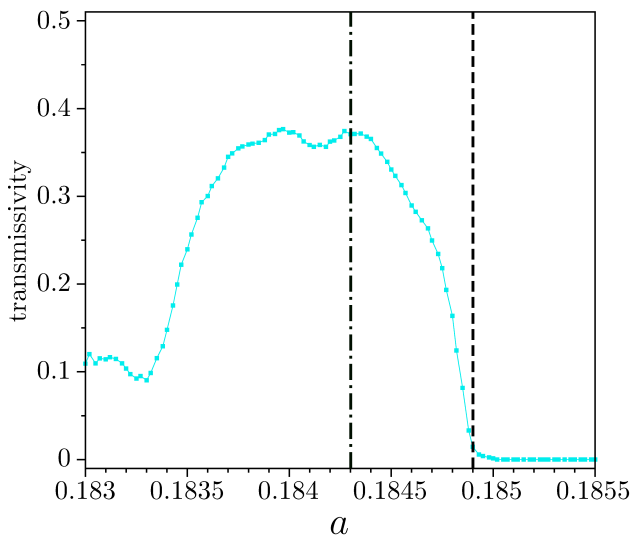


FIG. 8. Transmissivity of the Biquadratic Nontwist Map, as function of a , fixed $b = 0.77$ and $\varepsilon = 0.11$. Dashed-dotted and dashed lines mark high and low transport configurations, respectively. We iterated 10^5 initial conditions up to 10^6 times, considering boundaries at $y_B = 3.5$.

The escape time phase spaces of the high and low transmissivity configurations from Figure 8 are displayed in Figures 9(a) and 9(b), respectively. In both configurations, the transport barrier is characterized by an abrupt change in the average escape time, present only in the regions around $y \approx \pm 2.5$, corresponding to the external barriers. Beyond the external barriers orbits escape after a few iterations, while between them, orbits linger to escape. This orbit trapping is more effective in the low transmissivity scenario compared to the high transmissivity one, as evidenced by the average escape time of trapped orbits.

A detailed look at the escape times near the external barriers is shown in Figure 10, where we use the same parameters of high [Fig. 10(a)] and low [Fig. 10(b)] transmissivity configurations. A pair of isochronous island chains can be seen, whose remnants are responsible for the transport barrier.

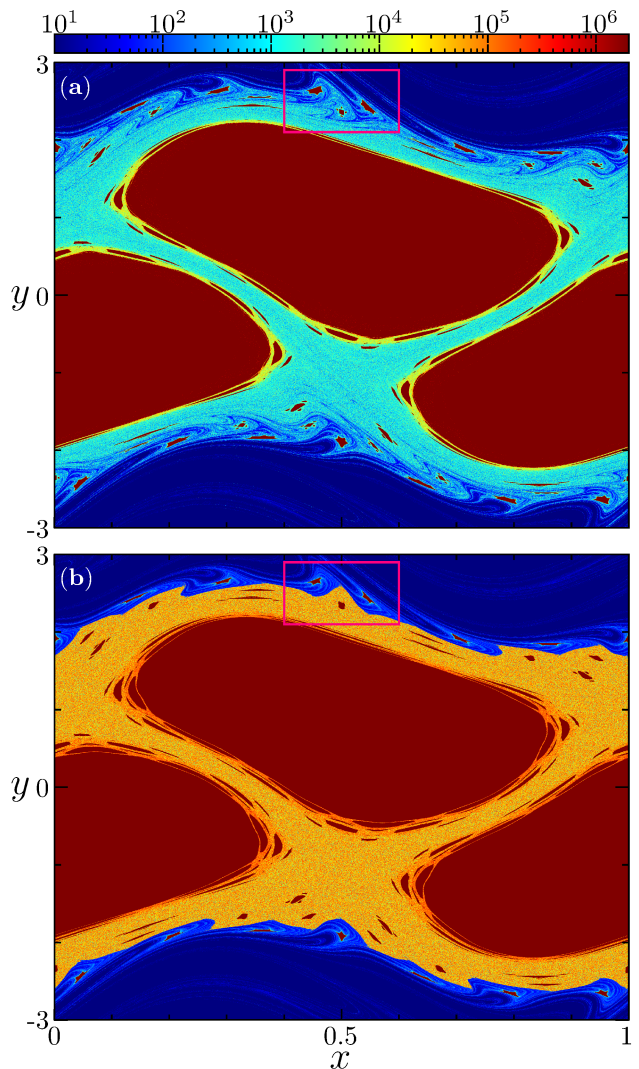


FIG. 9. Escape time of the trajectories in phase space of the Biquadratic Nontwist Map, with $b = 0.77$, $\varepsilon = 0.11$, (a) $a = 0.1843$ and (b) $a = 0.1849$, corresponding to high and low transport configurations of Fig. 8. Here we considered $y_B = 3.5$.

In opposition to the central transport barrier, the behavior of the map near the external barrier is asymmetric. Differences in upper and lower islands and in the average escape time are evident in Figure 10. In both low and high transport configurations, orbits take around 10^3 iterations to escape, except in the lower chain of low transport configuration, Figure 10(b). The finger-like structures in the escape time are present, dictating the escape channels of orbits. They are easily seen in Fig. 10(a); however, in the low transport regime (see Fig. 10(b)), they are only visible in the upper island chain due to the characteristic escape time of the region.

The associated hyperbolic manifolds also reflect the asymmetry of the map around the external island chain. Figure 11 shows the stable and unstable manifolds of the upper and lower island chain in Figure 10, denoted by $W_s^{U,L}$ and $W_u^{U,L}$.

Following the turnstile mechanism, manifolds typically have larger intercrossing lobes in the high transport regime.

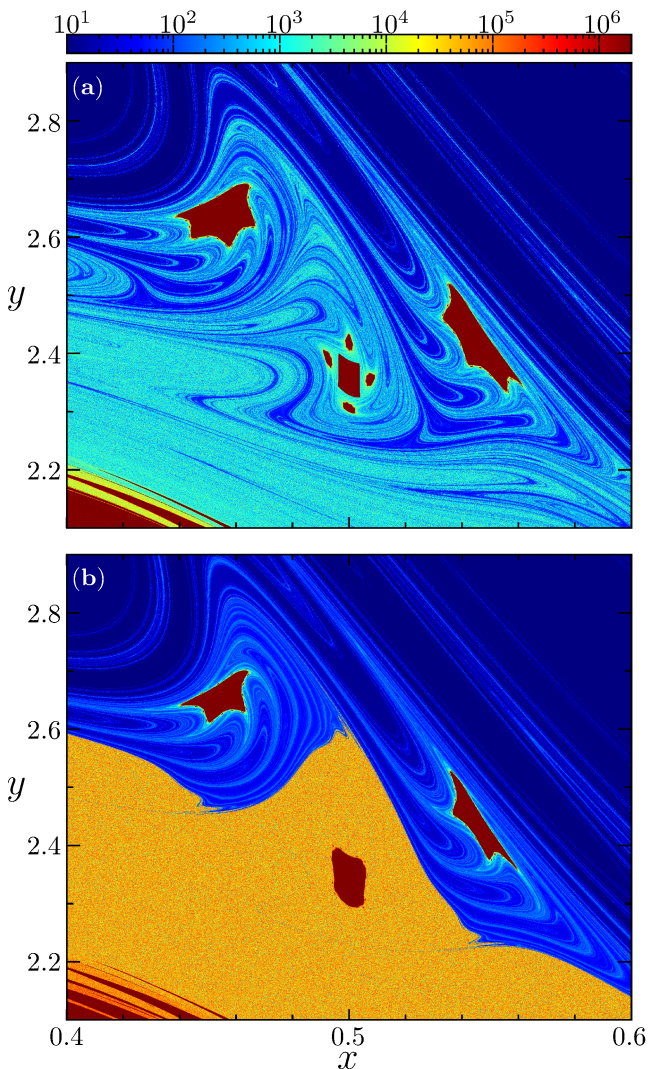


FIG. 10. Magnification of the highlighted rectangle in Fig. 9.

Nevertheless, an asymmetric behavior is evident when comparing the lower and upper orbits. The lobes of the lower manifolds have roughly the same size in both high and low transport regimes, as seen in Figures 11(a.2) and 11(b.2). Additionally, within the highlighted rectangle in Figure 11(b.2), small sized lobes are present. This asymmetry indicates an unequal upwards and downwards transmissivity of the transport barrier.

In the externally dominant scenario, high and low transmissivity is completely determined by intercrossing. Comparing Figures 11(a.3) and 11(b.3), we observed a prevalence of manifold intercrossing in the high transmissivity regime. Also, the hyperbolic manifolds appear to have a homoclinic-like topology when transmissivity is high. In this situation, upper (lower) manifolds intertwine with the lower (upper) chain, facilitating the interchange of orbits between pairs of isochronous island chains.

Examining manifold behavior (Fig. 11) and escape time (Fig. 10) we conclude that, in low transport regime, orbits easily enter and exit the resonance zone of the lower island

chain in the external barrier. However, due to the asymmetric behavior of manifolds, the probability of these orbits finding an escape channel leading from the lower to the upper chain is low.

V. CONCLUSION

In this paper, we investigated the transport properties in the Biquadratic Nontwist Map, a prototype of a nontwist system with multiple shearless curves. Although robust to perturbations, shearless curves eventually break up; however, their remnants continue to reduce transport in the region, forming effective transport barriers. The Biquadratic Nontwist Map presents three such regions of effective barriers, referred to as the central and external transport barriers.

We used two different dynamical quantifiers to characterize the effectiveness of transport barriers: the barrier transmissivity and the escape time of orbits. The first quantifier measures the fraction of orbits that overcome the transport barrier, regardless of the time needed. The second considers the time required for each orbit to escape from the barrier region. Our results indicate that the central and external transport barriers in the Biquadratic Nontwist Map have distinct effectiveness in two identified scenarios of dominance.

In the centrally dominant scenario, the transmissivity of the central transport barrier dominates over the external barriers. In this configuration, orbits shadow the behavior of island chains, trapping them into the barrier region. Conversely, in the externally dominant scenario, the central transport barrier offers almost no resistance to transport, and the external transport barriers play a major role. In this configuration, orbits are trapped between the two external transport barriers, with escape time substantially larger than untrapped orbits.

Complementarily, we examined manifold behavior in the two dominant scenarios. As expected, the qualitative nature of manifold crossing dictates the effectiveness of the partial barriers. High transport configurations, in both scenarios, are associated with manifold crossings of different island chains (intercrossing). However, since the map is asymmetric with respect to the external transport barriers, orbits crossing in this region have a preferred direction. This behavior is reflected in manifolds, which show varying-sized lobes.

In summary, our results indicate that the Biquadratic Nontwist Map exhibits complex transport properties due to the presence of multiple transport barriers. Each barrier has distinct transmissivity, leading to scenarios where either the central or external barriers dominate. The behavior of manifolds, especially their intercrossings, plays a critical role in determining the effectiveness of these barriers. Our findings suggest that in nontwist systems with multiple transport barriers, the interplay between these barriers creates regions in phase space with significant orbit trapping, influencing overall transport dynamics.

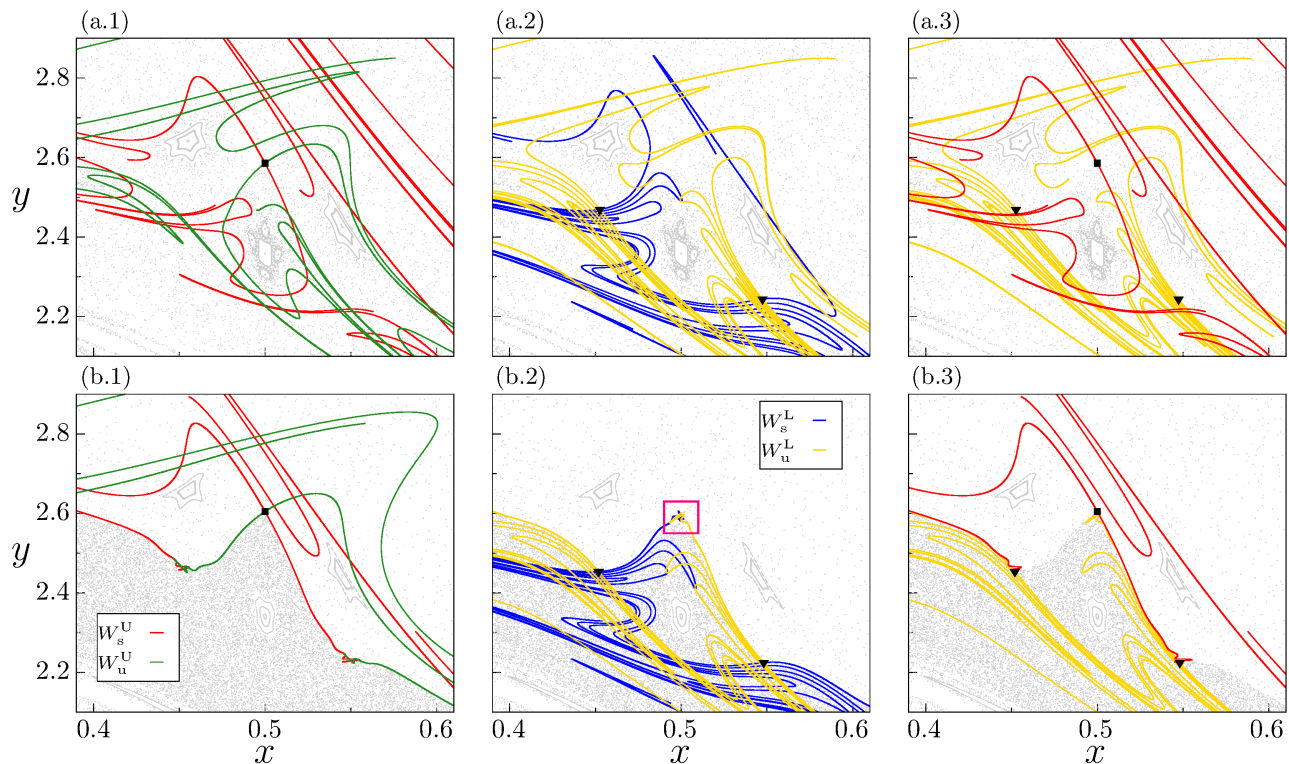


FIG. 11. Stable and unstable manifolds of the upper (W_s^U and W_u^U) and lower (W_s^L and W_u^L) periodic orbit, considering (a) high and (b) low transport configurations of Fig. 8. Chaotic orbits near them are plotted in light-grey.

ACKNOWLEDGMENTS

This research was initially supported by the National Council for Scientific and Technological Development (CNPq-Grant No. 309670/2023-3, 403120/2021-7 and 301019/2019-3) and Fundação de Amparo à Pesquisa do Estado de São Paulo (FAPESP) under Grants # 2018/03211-6, 2022/05667-2.

- ¹A. Wacker, “Semiconductor superlattices: a model system for nonlinear transport,” *Physics Reports* **357**, 1 (2002).
- ²W. S. Koon, M. W. Lo, J. E. Marsden, and S. D. Ross, “Heteroclinic connections between periodic orbits and resonance transitions in celestial mechanics,” *Chaos* **10**, 427 (2000).
- ³J. D. Meiss, “Thirty years of turnstiles and transport,” *Chaos* **25**, 097602 (2015).
- ⁴P. J. Morrison, “Hamiltonian description of the ideal fluid,” *Reviews of modern physics* **70**, 467 (1998).
- ⁵R. L. Viana, A. C. Mathias, L. C. Souza, and P. Haerter, “Fractal structures in the chaotic advection of passive scalars in leaky planar hydrodynamical flows,” *Chaos* **34** (2024).
- ⁶R. B. White and M. S. Chance, “Hamiltonian guiding center drift orbit calculation for plasmas of arbitrary cross section,” *Phys. Fluids* **27**, 2455 (1984).
- ⁷J. R. Cary and A. J. Brizard, “Hamiltonian theory of guiding-center motion,” *Reviews of modern physics* **81**, 693 (2009).
- ⁸A. H. Boozer, “Plasma equilibrium with rational magnetic surfaces,” *Phys. Fluids* **24**, 1999 (1981).
- ⁹R. L. Viana, M. Mugnaine, and I. L. Caldas, “Hamiltonian description for magnetic field lines in fusion plasmas: A tutorial,” *Physics of Plasmas* **30** (2023).
- ¹⁰J. D. Meiss, “Symplectic maps, variational principles, and transport,” *Rev. Mod. Phys.* **64**, 795 (1992).

- ¹¹R. S. MacKay, J. D. Meiss, and I. C. Percival, “Transport in Hamiltonian systems,” *Physica D* **13**, 55 (1984).
- ¹²J. Guckenheimer and P. Holmes, *Nonlinear oscillations, dynamical systems, and bifurcations of vector fields* (Springer - New York, 1983).
- ¹³I. I. Rypina, M. G. Brown, F. J. Beron-Vera, H. Koçak, M. J. Olascoaga, and I. A. Udovychenkov, “Robust transport barriers resulting from strong Kolmogorov-Arnold-Moser stability,” *Physical Review Letters* **98**, 104102 (2007).
- ¹⁴D. del Castillo-Negrete, J. M. Greene, and P. J. Morrison, “Area preserving nontwist maps: periodic orbits and transition to chaos,” *Physica D* **91**, 1 (1996).
- ¹⁵R. Egydio de Carvalho and A. M. Ozorio de Almeida, “Integrable approximation to the overlap of resonances,” *Physics Letters A* **162**, 457 (1992).
- ¹⁶A. Wurm, A. Apte, K. Fuchss Portela, and P. Morrison, “Meanders and reconnection–collision sequences in the standard nontwist map,” *Chaos* **15**, 023108 (2005).
- ¹⁷G. Corso and F. B. Rizzato, “Manifold reconnection in chaotic regimes,” *Phys. Rev. E* **58**, 8013 (1998).
- ¹⁸M. Mugnaine, A. C. Mathias, M. S. Santos, A. M. Batista, J. D. Szezech Jr, and R. L. Viana, “Dynamical characterization of transport barriers in nontwist hamiltonian systems,” *Physical Review E* **97**, 012214 (2018).
- ¹⁹M. Mugnaine, J. D. Szezech Jr, R. L. Viana, I. L. Caldas, and P. J. Morrison, “Shearless effective barriers to chaotic transport induced by even twin islands in nontwist systems,” *arXiv preprint arXiv:2406.19947* (2024).
- ²⁰J. D. Szezech, I. L. Caldas, S. R. Lopes, R. L. Viana, and P. J. Morrison, “Transport properties in nontwist area-preserving maps,” *Chaos* **19**, 043108 (2009).
- ²¹D. del Castillo-Negrete and P. J. Morrison, *Physics of Fluids A* **5**, 948 (1993).
- ²²D. del Castillo-Negrete, “Chaotic transport in zonal flows in analogous geophysical and plasma systems,” *Phys. Plasmas* **7**, 1702 (2000).
- ²³I. L. Caldas, R. L. Viana, C. V. Abud, J. D. da Fonseca, Z. O. Guimarães Filho, and T. Kroetz *et al.*, “Shearless transport barriers in magnetically confined plasmas,” *Plasma Phys. Control. Fusion* **54**, 124035 (2012).

- ²⁴P. J. Morrison, “Magnetic field lines, Hamiltonian dynamics, and nontwist systems,” *Phys. Plasmas* **7**, 2279 (2000).
- ²⁵R. F. Gandy, G. J. Hartwell, J. D. Hanson, S. Knowlton, and H. Lin, “An experimental study of magnetic islands as hamiltonian systems,” *Physics of Fluids B* **5**, 4384 (1993).
- ²⁶M. G. Davidson, R. L. Dewar, H. J. Gardner, and J. Howard, “Hamiltonian maps for Helic magnetic islands,” *Australian Journal of Physics* **48**, 871 (1995).
- ²⁷R. Dewar and J. Meiss, “Flux-minimizing curves for reversible area-preserving maps,” *Physica D* **57**, 476 (1992).
- ²⁸R. Dewar, S. Hudson, and P. Price, “Almost invariant manifolds for divergence-free fields,” *Physics Letters A* **194**, 49 (1994).
- ²⁹R. Dewar and A. Khorev, “Rational quadratic-flux minimizing circles for area-preserving twist maps,” *Physica D* **85**, 66 (1995).
- ³⁰D. Constantinescu, J. Misguich, I. Pavlenko, and E. Petrisor, “Internal transport barriers in some hamiltonian systems modeling the magnetic lines dynamics in tokamak,” *Journal of Physics: Conference Series* **7**, 233 (2005).
- ³¹J. S. Portela, I. L. Caldas, R. L. Viana, and M. A. F. Sanjuan, “Fractal and Wada exit basin boundaries in tokamaks,” *International Journal of Bifurcation and Chaos* **17**, 4067 (2007).
- ³²J. D. Szezech, I. L. Caldas, S. R. Lopes, P. J. Morrison, and R. L. Viana, “Effective transport barriers in nontwist systems,” *Phys. Rev. E* **86**, 036206 (2012).
- ³³M. Farazmand, D. Blazeovski, and G. Haller, “Shearless transport barriers in unsteady two-dimensional flows and maps,” *Physica D* **278**, 44 (2014).
- ³⁴E. Joffrin, C. Challis, G. Conway, X. Garbet, A. Gude, S. Günter, N. Hawkes, T. Hender, D. Howell, G. Huysmans, *et al.*, “Internal transport barrier triggering by rational magnetic flux surfaces in tokamaks,” *Nuclear Fusion* **43**, 1167 (2003).
- ³⁵G. C. Grime, M. Roberto, R. L. Viana, Y. Elskens, and I. L. Caldas, “Shearless bifurcations in particle transport for reversed-shear tokamaks,” *J. Plasma Phys.* **89**, 835890101 (2023).
- ³⁶D. del Castillo-Negrete and J. J. Martinell, “Gyroaverage effects on non-twist Hamiltonians: Separatrix reconnection and chaos suppression,” *Commun. Nonlinear Sci. Numer. Simul.* **17**, 2031 (2012).
- ³⁷J. D. Fonseca, D. del Castillo-Negrete, and I. L. Caldas, “Area-preserving maps models of gyroaveraged $E \times B$ chaotic transport,” *Phys. Plasmas* **21**, 092310 (2014).
- ³⁸J. E. Howard and J. Humpherys, “Nonmonotonic twist maps,” *Physica D* **80**, 256 (1995).
- ³⁹G. C. Grime, M. Roberto, R. L. Viana, Y. Elskens, and I. L. Caldas, “Biquadratic nontwist map: a model for shearless bifurcations,” *Chaos, Solitons & Fractals* **169**, 113231 (2023).
- ⁴⁰G. C. Grime, M. Roberto, R. L. Viana, Y. Elskens, and I. L. Caldas, “Shearless curve breakup in the biquadratic nontwist map,” *Chaos, Solitons & Fractals* **172**, 113606 (2023).
- ⁴¹L. E. Reichl, *Transition to Chaos: conservative classical systems and quantum manifestations*, 2nd ed. (Springer Verlag - New York, 2004).
- ⁴²A. J. Lichtenberg and M. A. Lieberman, *Regular and Chaotic Dynamics*, 2nd ed. (Springer Verlag - New York, 1992).
- ⁴³J. E. Howard and S. M. Hohns, “Stochasticity and reconnection in Hamiltonian systems,” *Phys. Rev. A* **29**, 418 (1984).
- ⁴⁴E. Petrisor, “Nontwist area preserving maps with reversing symmetry group,” *Int. J. Bifurcat. Chaos* **11**, 497 (2001).
- ⁴⁵K. Fuchss Portela, A. Wurm, A. Apte, and P. Morrison, “Breakup of shearless meanders and “outer” tori in the standard nontwist map,” *Chaos* **16**, 033120 (2006).
- ⁴⁶B. V. Chirikov and D. L. Shepelyansky, “Asymptotic statistics of poincaré recurrences in hamiltonian systems with divided phase space,” *Physical Review Letters* **82**, 528 (1999).
- ⁴⁷D. Ciro, I. L. Caldas, and T. E. Evans, “Efficient manifolds tracing for planar maps,” *Chaos* **28**, 093106 (2018).